

Theory for doping trends in titanium oxypnictide superconductors

Han-Xiang Xu,¹ Daniel Guterding,² and Harald O. Jeschke¹

¹Research Institute for Interdisciplinary Science, Okayama University, Okayama 700-8530, Japan

²Fachbereich Mathematik, Naturwissenschaften und Datenverarbeitung,

Technische Hochschule Mittelhessen, Wilhelm-Leuschner-Straße 13, 61169 Friedberg, Germany

(Dated: December 2, 2021)

A family of titanium oxypnictide materials $\text{BaTi}_2Pn_2\text{O}$ ($Pn = \text{pnictogen}$) becomes superconducting when a charge and/or spin density wave is suppressed. With hole doping, isovalent doping and pressure, a whole range of tuning parameters is available. We investigate how charge doping controls the superconducting transition temperature T_c . To this end, we use experimental crystal structure data to determine the electronic structure and Fermi surface evolution along the doping path. We show that a naive approach to calculating T_c via the density of states at the Fermi level and the McMillan formula systematically fails to yield the observed T_c variation. On the other hand, spin fluctuation theory pairing calculations allow us to consistently explain the T_c increase with doping. All alkali doped materials $\text{Ba}_{1-x}A_x\text{Ti}_2\text{Sb}_2\text{O}$ ($A=\text{Na, K, Rb}$) are described by a sign-changing s -wave order parameter. Susceptibilities also reveal that the physics of the materials is controlled by a single Ti $3d$ orbital.

Introduction.- The first layered titanium oxypnictides $\text{Na}_2\text{Ti}_2\text{As}_2\text{O}$ and $\text{Na}_2\text{Ti}_2\text{Sb}_2\text{O}$ were synthesized three decades ago [1] and discussed in terms of spin density wave (SDW) or charge density wave (CDW) behavior [2, 3]. Nine years ago, superconductivity was discovered in $\text{BaTi}_2\text{Sb}_2\text{O}$ [4] and $\text{BaTi}_2\text{Bi}_2\text{O}$ [5]. By analysis of the $\text{BaTi}_2(\text{As}_{1-x}\text{Sb}_x)_2\text{O}$ solid solutions it quickly became apparent that superconductivity is favored by a suppression of the CDW/SDW phase [6, 7]. An extensive discussion of the phase transition observed in resistivity and magnetic susceptibility [2, 4, 8, 9] as well as thermoelectric power and Hall coefficient [10] concerns the question whether it should be characterized as a CDW transition or if it is in fact an SDW transition. Experimental evidence from nuclear magnetic resonance (NMR) [11] and muon spin relaxation (μSR) [12, 13] does not completely resolve the question.

Shortly after the discovery of superconductivity, it was realized that both charge doping on the barium site and isovalent doping on the pnictogen site provide opportunities to control the superconductivity of $\text{BaTi}_2\text{Sb}_2\text{O}$ in a significant range. Hole doping via alkali metals increases T_c from 1.2 K to 5.5 K in $\text{Ba}_{1-x}\text{Na}_x\text{Ti}_2\text{Sb}_2\text{O}$ [9, 12], to 6.1 K in $\text{Ba}_{1-x}\text{K}_x\text{Ti}_2\text{Sb}_2\text{O}$ [14], to 5.4 K in $\text{Ba}_{1-x}\text{Rb}_x\text{Ti}_2\text{Sb}_2\text{O}$ [15] and to 4.4 K in $\text{Ba}_{1-x}\text{Cs}_x\text{Ti}_2\text{Sb}_2\text{O}$ [16]. The maximum T_c is reached near an alkali content of $x = 0.2$ to 0.3 . Isovalent doping via Sb/Bi mixing yields an intriguing two-dome T_c evolution with a non-superconducting or low T_c phase in between [6, 17]. More recently, pressure has been demonstrated to be an effective control parameter for superconductivity [18].

The nature of superconductivity in the titanium oxypnictides has been discussed since its discovery [19]. Experimentally, an s -wave gap has been inferred from nuclear quadrupole resonance (NQR) measurements [11], and specific heat is partially consistent with BCS expectations [20]. However, μSR measurements have been taken to indicate an unconventional pairing mech-

anism [21]. An NMR/NQR study points to significant differences in the superconductivity of $\text{BaTi}_2\text{Sb}_2\text{O}$ and $\text{BaTi}_2\text{Bi}_2\text{O}$ [22].

Theoretically, calculations of electron-phonon coupling have shown that the small transition temperature of $\text{BaTi}_2\text{Sb}_2\text{O}$ can be explained by an electron-phonon mechanism [23]. On the other hand, based on the Fermi surfaces a sign-changing s -wave state has been predicted within spin fluctuation theory [24]. While the presence of magnetism has not been fully established in the titanium oxypnictides, an extensive density functional theory (DFT) study and symmetry analysis of the nematicity and charge order in $\text{BaTi}_2\text{Sb}_2\text{O}$ have provided strong evidence that these materials cannot be understood without taking spin fluctuations into account [25].

While the electronic structure of individual titanium oxypnictide metals [26, 27] and superconductors [24, 28, 29] has been studied repeatedly, there is no theory for the evolution of properties with doping. Our study is intended to fill this gap. In this work, we show that we can consistently explain the evolution of the superconducting T_c with alkali doping using spin fluctuation theory and that the superconducting gap function has a sign-changing s -wave symmetry.

Methods.- We perform electronic structure calculations using the full potential local orbital (FPLO) basis set [30] and generalized gradient approximation (GGA) to the exchange and correlation potential [31]. We use smooth interpolations of lattice parameters of the $P4/mmm$ space group (see Appendix A, Fig. 7) and optimize the antimony positions within GGA. The charge doping is modeled via the virtual crystal approximation on the barium site. We use projective Wannier functions within FPLO [32] to obtain 26 band tight binding models including Ti $3d$ and $4s$, Ba $5d$, Sb $5p$ and O $2p$ orbital characters. The models follow DFT bands and Fermi surfaces to a high degree of accuracy (see Appendix B, Fig. 8). Based on the tight binding model, we calculate non-interacting susceptibilities $\chi_{st}^{pq}(\mathbf{q})$. We apply

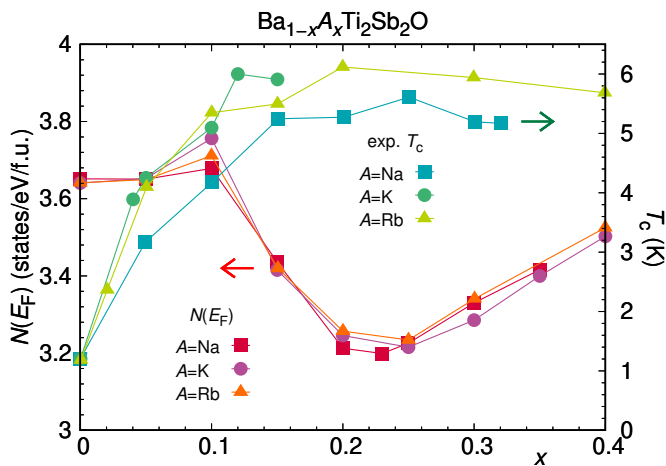


FIG. 1. Density of states at the Fermi level $N(E_F)$ shown together with experimental superconducting transition temperatures T_c for doping with three different alkali ions. T_c data are from Ref. 9 and 20 for Na doping, Ref. 14 for K doping, Ref. 15 for Rb doping.

the random phase approximation (RPA) and investigate the pairing instabilities within spin fluctuation theory by solving the gap equation on the Fermi surface [33–36] (for details, see Appendix D). Interaction parameters of $U = 2$ eV (intra-orbital Coulomb repulsion), $U' = 1$ eV (inter-orbital Coulomb repulsion), $J = 0.5$ eV (Hund’s rule coupling) and $J' = 0.5$ eV (pair hopping), applied to Ti $3d$ orbitals, were used for RPA and pairing calculations. Note that a limitation of RPA based fluctuation theory is the restriction to zero energy, and application of the fluctuation exchange approximation (FLEX) which takes the energy dependence into account is an interesting future extension of our study.

Results.— The titanium oxypnictide superconductors have been treated as simple Bardeen, Cooper, Shrieffer (BCS) type superconductors in various experimental [4, 11, 15, 20, 37] and theoretical [23] studies. As a straight-forward attempt to understand the T_c tendencies, we extract the density of states at the Fermi level $N(E_F)$ as a function of doping and try to apply the BCS formula $T_c = 1.134 T_D \exp\left(-\frac{1}{VN(E_F)}\right)$ (with Debye temperature T_D and electron-phonon coupling potential V). Assuming constant T_D and V , this formula and its more sophisticated variants yield T_c trends that essentially follow $N(E_F)$. Note that our use of the virtual crystal approximation is justified by good comparison of our Fermi surfaces to angle resolved photoemission (see Appendix C, Fig. 10). Nevertheless, conducting a similar study based on a more elaborate approach for treating alkali doping and Ba/alkali site disorder like the coherent potential approximation will be an interesting future endeavor.

Unfortunately, as Fig. 1 shows, there is very little similarity between $N(E_F)$ and T_c evolution with doping. In the case of alkali doping of $\text{BaTi}_2\text{Sb}_2\text{O}$, T_c quickly increases from $T_c = 1.2$ K to a maximum that is reached

between doping levels of $x = 0.1$ to 0.3 . Meanwhile, $N(E_F)$ remains constant until $x = 0.1$ before going through a minimum at $x = 0.23$ (Fig. 1). Based on this analysis, superconductivity in these materials could only be explained by an electron-phonon mechanism if the strength of electron-phonon coupling was extremely doping-dependent, so that it counteracts the unhelpful trends in $N(E_F)$. However, this seems very far-fetched because in the small doping range considered, neither T_D nor V are expected to vary strongly. Therefore, we now turn to the possibility that the detailed evolution of the Fermi surface nesting provides doping dependencies strong enough to explain the evolution of T_c within spin fluctuation pairing theory. So far, the charge density wave state has been studied with spin fluctuation theory including Aslamazov-Larkin vertex corrections [38] or within dynamical mean field theory [39] but only a limited study of superconductivity exists [28].

First, we identify the most relevant orbitals at the Fermi level. In Fig. 2(a), we show the band structure and density of states of $\text{BaTi}_2\text{Sb}_2\text{O}$ with Ti $3d$ and Sb $5p$ orbital character highlighted. The system is in general quite strongly hybridized and many orbitals contribute to the states close to the Fermi level. Taking a closer look, we find that the most relevant Ti $3d$ orbital for the low energy physics is $3d_{xy}$ followed by $3d_{xz,yz}$. To visualize the Ti $3d_{xy}$ orbital, we choose a local coordinate system for Ti where the z -axis points along the Ti-O bond and x - and y -axes point along Ti-Sb bonds. This is the natural local system to choose within the TiO_2Sb_4 octahedron [27] (Fig. 2(b)), since it makes $3d_{xz}$ and $3d_{yz}$ degenerate. Fig. 2(c) shows the $3d_{xy}$ Wannier functions at both titanium sites (Ti1 and Ti2) based on this coordinate choice.

We now analyze the Fermi surface evolution with alkali doping (Fig. 3). Only Ti $3d_{xy}$ and Sb $5p$ weights are highlighted (see Appendix C, Fig. 9 for the other $3d$ weights). Note that focusing on Ti and Sb is justified because relative contributions to the density of states at the Fermi level $N(E_F)$ are 74%, 20%, 4% and 1% for Ti, Sb, Ba and O, respectively. The $\text{BaTi}_2\text{Sb}_2\text{O}$ Fermi surface is in excellent agreement with angle resolved photoemission (ARPES) experiments [40, 41] (see Appendix C, Fig. 10). We see that the hole Fermi surfaces at X and Y grow with doping while the electron Fermi surface at M shrinks slightly. The Fermi surface at Γ , which is dominated by Sb $5p$, shows a rather complicated reconstruction as a function of doping. This can be understood by tracing which orbital fillings are depleted by the holes introduced as function of alkali doping level x . In fact, the majority of doped holes are in Sb orbitals while Ti $3d$ orbitals are nearly unaffected. The changes seen in Fermi surfaces with Ti $3d$ character (Fig. 3) are due to stronger Sb-Ti bonding upon hole doping rather than due to a Fermi level shift.

In order to measure the relative importance of the Fermi surface changes, we turn to non-interacting susceptibilities calculated with the 26 band tight binding

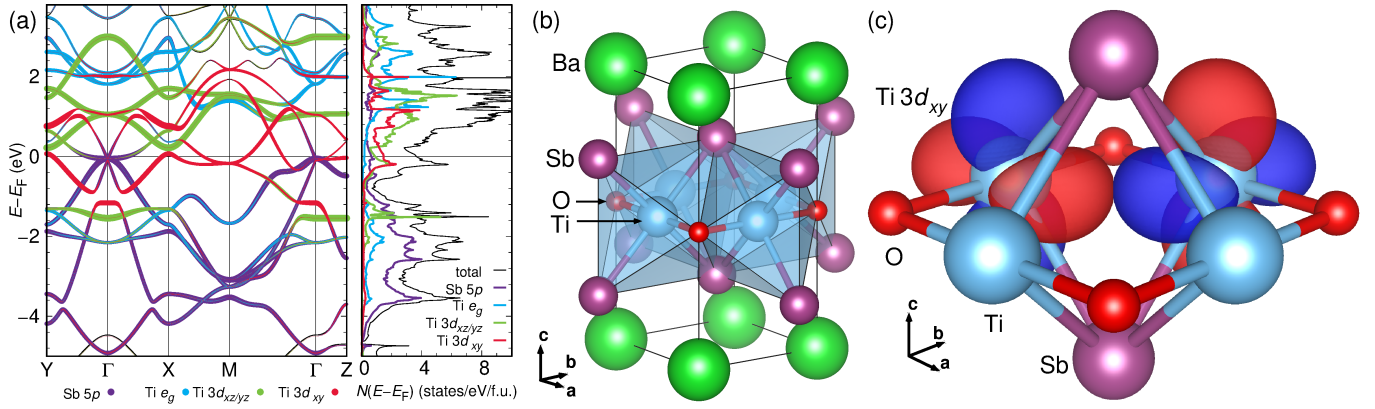


FIG. 2. (a) GGA band structure and density of states of $\text{BaTi}_2\text{Sb}_2\text{O}$. (b) Crystal structure of $\text{BaTi}_2\text{Sb}_2\text{O}$ with shaded TiO_2Sb_4 octahedra. (c) $\text{Ti } 3d_{xy}$ Wannier functions within the $\text{Ti}_2\text{Sb}_2\text{O}$ layer of $\text{BaTi}_2\text{Sb}_2\text{O}$.

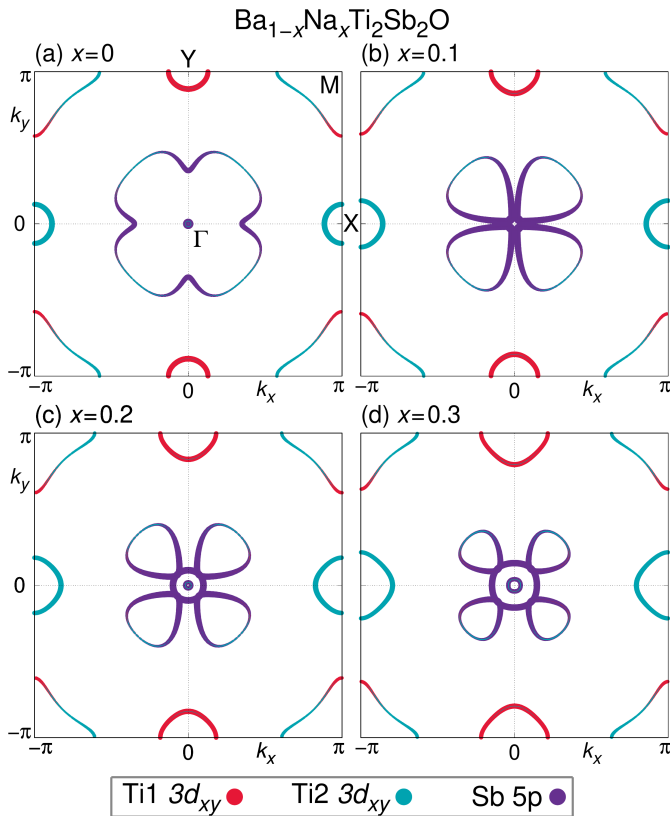


FIG. 3. Fermi surfaces of $\text{Ba}_{1-x}\text{Na}_x\text{Ti}_2\text{Sb}_2\text{O}$ at $k_z = 0$ as function of doping level x , calculated within GGA.

models on $50 \times 50 \times 50$ integration meshes. Fig. 4 shows that the total susceptibility χ_0 is clearly peaked at $\mathbf{q} = (\pi, 0, 0)$ (labeled X) and $\mathbf{q} = (0, \pi, 0)$ (labeled Y). Previously, this has been noted based on the Lindhard function calculated without matrix elements [24, 28]. With alkali doping, the peaks at X and Y decrease, and they also move away from the high symmetry point towards Γ . At the same time, χ_0 at $\mathbf{q} = (0, 0, 0)$ decreases. Interestingly, the doping trends of the total χ_0 and χ_0^{xy}

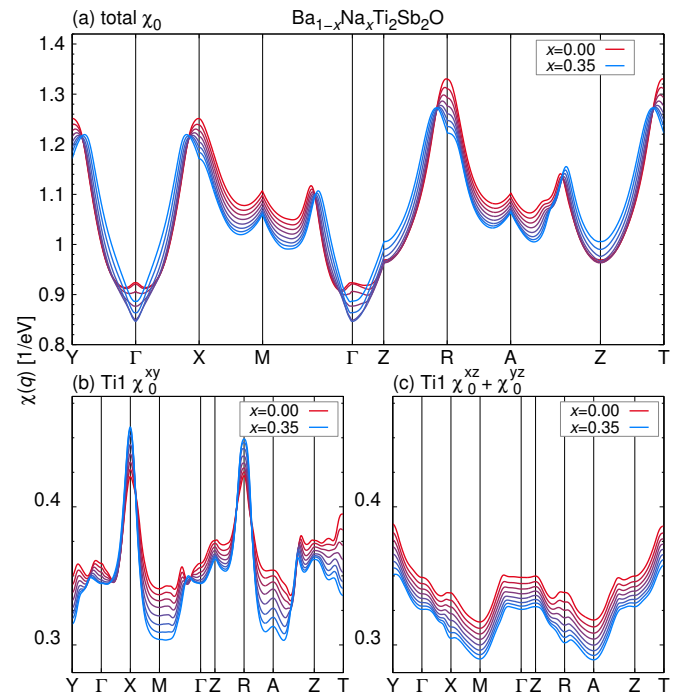


FIG. 4. Non-interacting susceptibility of $\text{Ba}_{1-x}\text{Na}_x\text{Ti}_2\text{Sb}_2\text{O}$ for eight doping levels x . (a) total, (b) $3d_{xy}$ contribution from Ti1, (c) $3d_{xz}$ and $3d_{yz}$ contributions from Ti1. $\mathbf{q} = (\pi, 0, 0)$ is labeled as X , $\mathbf{q} = (0, \pi, 0)$ as Y , $\mathbf{q} = (\pi, \pi, 0)$ as M , $\mathbf{q} = (0, 0, \pi)$ as Z , $\mathbf{q} = (0, \pi, \pi)$ as R , $\mathbf{q} = (\pi, \pi, \pi)$ as A and $\mathbf{q} = (\pi, 0, \pi)$ as T .

differ: While the ratio between X and Γ values of χ_0 hardly changes with doping, this ratio sharply increases for χ_0^{xy} due to increases at X combined with decreases at Γ . This improved nesting is shown in Fig. 4 (b) for Ti1, but equally applies to Ti2 where the Y to Γ ratio increases sharply. Furthermore, even though the Fermi surface shows substantial k_z dispersion, we can find the improved nesting also in the R to Z ratio. Meanwhile, the other orbitals, which are of some significance at the Fermi

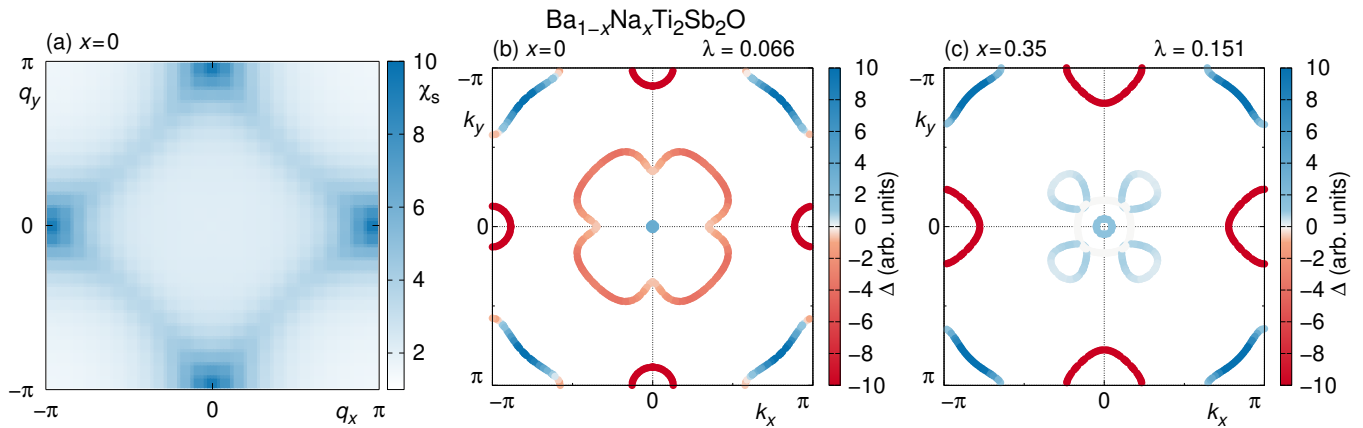


FIG. 5. Two-dimensional susceptibility and gap functions of $\text{Ba}_{1-x}\text{Na}_x\text{Ti}_2\text{Sb}_2\text{O}$. (a) Spin susceptibility χ_s calculated within RPA for $x = 0$, showing enhanced maxima at $\mathbf{q} = (0, \pi)$ and $\mathbf{q} = (\pi, 0)$. (b) and (c) Eigen functions for the leading eigenvalue of the gap equation at zero doping and at maximal doping. The sign-changing s -wave persists at all doping levels.

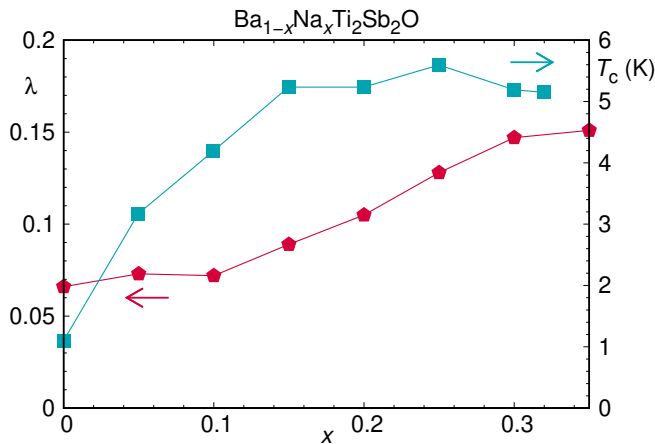


FIG. 6. Leading eigenvalues λ of the gap equation as a function of doping level x . T_c data are from Ref. 9 and 20.

level ($3d_{xz}$ and $3d_{yz}$), have a comparatively featureless susceptibility (Fig. 4(c)) which uniformly decreases with doping. It is justified to focus on Ti $3d$ susceptibilities here because the Sb susceptibilities are small, almost flat with respect to \mathbf{q} and they grow even more featureless with doping (see Fig. 11). Note that calculations without matrix elements, i.e. solely based on the Lindhard function, do not contain the orbital-resolved information we just discussed. Since alkali doping seems to lead to an overall decrease in susceptibility, but strongly enhances the susceptibility of the Ti $3d_{xy}$ orbitals, we can expect them to be the main actor in T_c changes with doping.

Since the similarity of susceptibilities along the $k_z = 0$ and $k_z = \pi$ paths in Fig. 4(a) indicates a high degree of two-dimensionality, we now focus on the $k_z = 0$ cuts of susceptibility and pairing in Fig. 5. It is clear that features of the non-interacting susceptibility χ_0 (see Appendix E, Fig. 12), especially peaks at $\mathbf{q} = (\pi, 0)$ and $\mathbf{q} = (0, \pi)$, are enhanced in the interacting susceptibility obtained by random phase approximation (Fig. 5(a)),

reminiscent of single orbital system behaviour. These instabilities would now favor stripe-type magnetism which, however, has not been observed for $\text{BaTi}_2\text{Sb}_2\text{O}$ [11–13].

Here, the $(\pi, 0)$ and $(0, \pi)$ instabilities favor a sign-changing s -wave superconducting order parameter: The gap functions corresponding to the leading eigenvalue λ , obtained using spin fluctuation theory, are shown in Fig. 5(b) and (c) for two different doping levels. Subleading d_{xy} - and $d_{x^2-y^2}$ -type solutions have far smaller eigenvalues and are, therefore, irrelevant in $\text{Ba}_{1-x}\text{Na}_x\text{Ti}_2\text{Sb}_2\text{O}$. The eigenvalue λ increases as a function of alkali doping (Fig. 6), and follows the doping trend of the maxima in the susceptibility (Fig. 4(a)). Thus, the increase of T_c with alkali doping (Fig. 1) is clearly explained by the susceptibility trends rather than the density of states at the Fermi level. By performing the pairing calculations on 3D Fermi surfaces, we have verified that the sign-changing s -wave is indeed the dominating solution for all alkali doped materials $\text{Ba}_{1-x}\text{A}_x\text{Ti}_2\text{Sb}_2\text{O}$ ($\text{A}=\text{Na}, \text{K}, \text{Rb}$).

At low alkali doping levels we have found an order parameter, which contains nodes on the Fermi surface sheets around M and a relatively large gap on the central Fermi surface sheets around Γ . With increasing doping, the Fermi surface sheets around M become nodeless, but the reconstructed sheets around Γ , which are almost exclusively of Sb $5p$ character, are hardly gapped at all. Those strongly non-uniform order parameters need to be taken into account when interpreting thermodynamic and other experiments trying to determine the symmetry of the superconducting state in titanium oxypnictides.

Conclusions.— We have investigated the electronic and superconducting properties of $\text{Ba}_{1-x}\text{Na}_x\text{Ti}_2\text{Sb}_2\text{O}$ using density functional and spin fluctuation theory. We modeled the crystal structure evolution using an interpolation of experimental lattice parameters and a DFT predicted antimony position. The density of states at the Fermi level $N(E_F)$ shows a trend which is in sharp contrast to the evolution of the superconducting T_c , indicating that

transition temperatures may not be accounted for by an electron-phonon mechanism.

Although the band structure and density of states show that constituents of $\text{Ba}_{1-x}\text{A}_x\text{Ti}_2\text{Sb}_2\text{O}$ ($\text{A}=\text{Na}, \text{K}, \text{Rb}$) are strongly hybridized and many orbitals lie close to the Fermi level, we have found that the susceptibility is completely dominated by the Ti $3d_{xy}$ orbitals.

Proceeding on the assumption of a magnetic pairing mechanism, which has been suggested by an investigation into the nematicity of $\text{BaTi}_2\text{Sb}_2\text{O}$ in Ref. 25, we find that we can satisfactorily explain the T_c trend with a spin fluctuation pairing mechanism. We find that a sign-changing s -wave order parameter with non-uniform gap size on the various Fermi surface sheets clearly dominates in $\text{Ba}_{1-x}\text{Na}_x\text{Ti}_2\text{Sb}_2\text{O}$ at all doping levels. Explaining the nontrivial transition temperature trends of titanium based superconductors with isoelectronic doping and pressure are interesting future fields of study. Methodologically, it may be important to consider also the energy dependence within the fluctuation exchange approximation (FLEX).

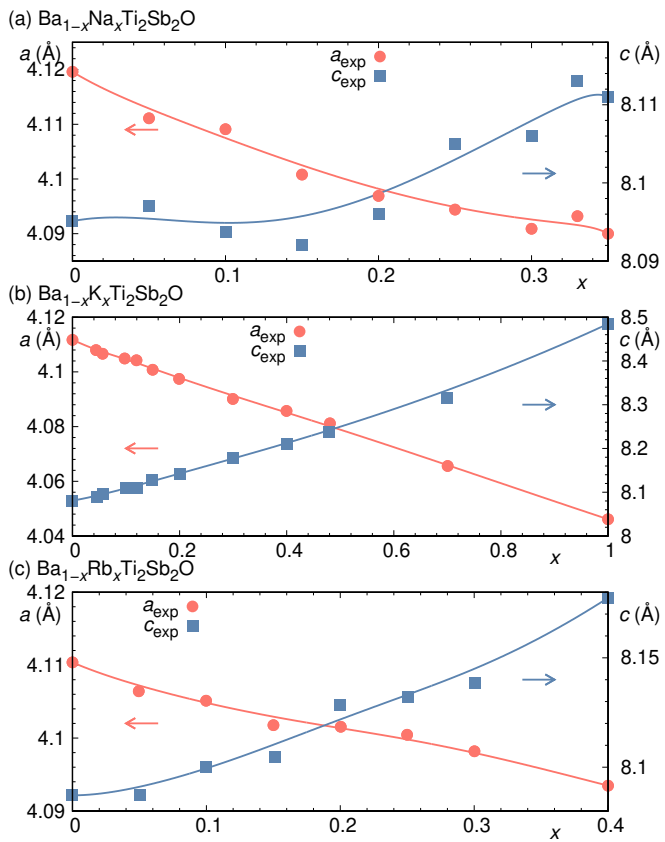


FIG. 7. Interpolation of experimental lattice constants.

Appendix A: Crystal structures

We use experimental lattice parameters for $\text{Ba}_{1-x}\text{Na}_x\text{Ti}_2\text{Sb}_2\text{O}$ from Ref. 9, for $\text{Ba}_{1-x}\text{K}_x\text{Ti}_2\text{Sb}_2\text{O}$

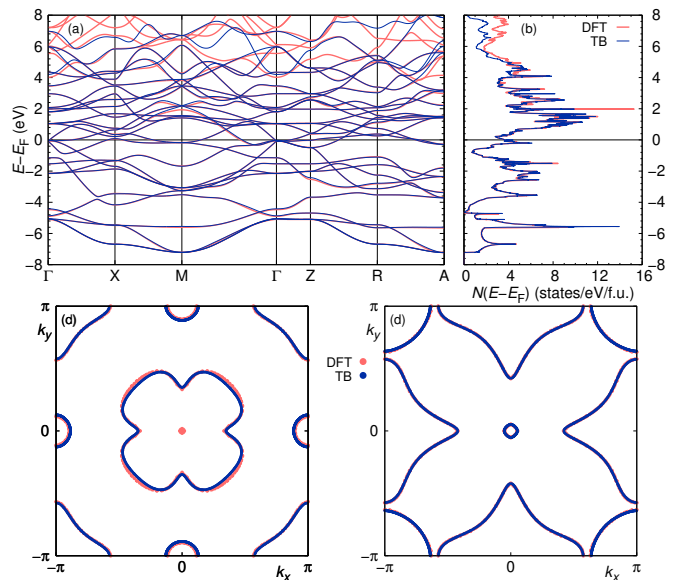


FIG. 8. Comparison between density functional theory and tight binding model for $\text{BaTi}_2\text{Sb}_2\text{O}$. (a) Band structure, (b) density of states, (c) Fermi surface at $k_z = 0$ and (d) Fermi surface at $k_z = \pi$. The agreement is excellent.

from Ref. 14 and for $\text{Ba}_{1-x}\text{Rb}_x\text{Ti}_2\text{Sb}_2\text{O}$ from Ref. 15. They are shown as symbols in Fig. 7. We smoothly

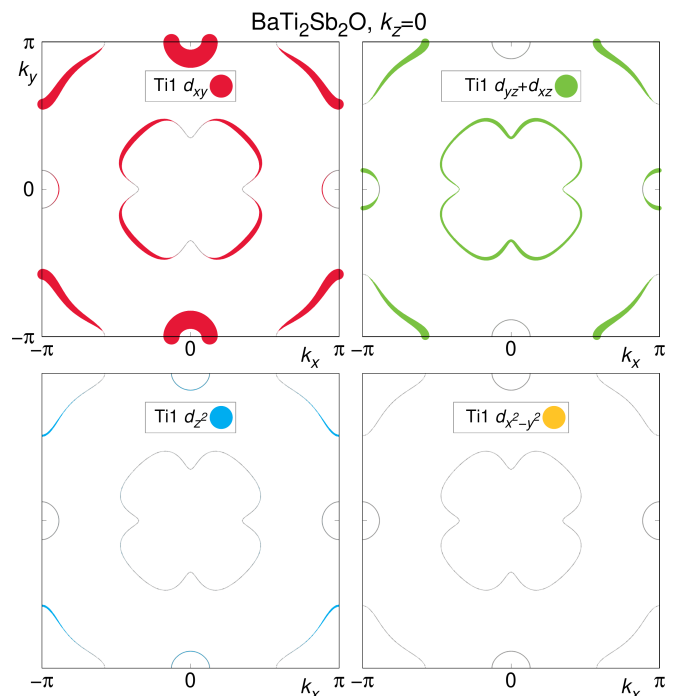


FIG. 9. 2D Fermi surface of $\text{BaTi}_2\text{Sb}_2\text{O}$ with Ti $3d$ orbital character. All weights are shown with the same scale. $3d_{xy}$ clearly dominates, followed in importance by $3d_{yz}/3d_{xz}$. $3d_{z^2}$ is very faint, and $3d_{x^2-y^2}$ character is negligible. Weights of the second Ti site are 90 degree rotated with respect to the first so that the sum has the C_4 symmetry of the space group.

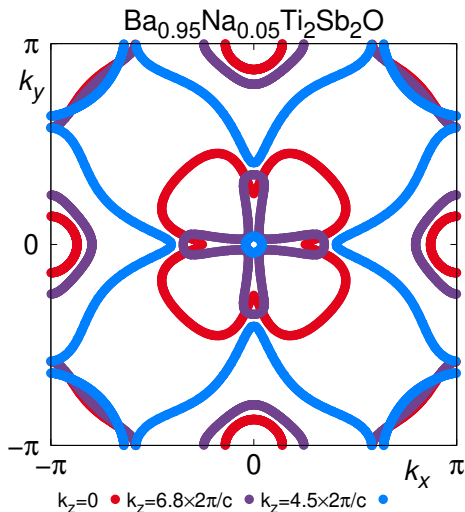


FIG. 10. Fermi surface of $\text{Ba}_{0.95}\text{Na}_{0.05}\text{Ti}_2\text{Sb}_2\text{O}$ at $k_z = 0$, $k_z = 0.5\pi$ and $k_z = \pi$, calculated within GGA.

interpolate the lattice parameters in order to sample the doped crystal structures at regular intervals. Note that in the case of the c lattice parameter of $\text{Ba}_{1-x}\text{Na}_x\text{Ti}_2\text{Sb}_2\text{O}$ where the experimental lattice constants are rather nonmonotonous, the overall scale of the variation is small; as there is little justification for a dramatic doping dependence, we expect that the slight smoothing due to the interpolation is reducing error rather than losing detail. The antimony positions are the only free positions in the $P4/mmm$ crystal structures, and we obtain them by relaxation using FPLO basis [30] and GGA exchange correlation functional. Note that for the experimentally known $\text{BaTi}_2\text{Sb}_2\text{O}$ structure the deviation in Ti-Sb distance and Sb-Ti-Sb angle is only 0.2% for the relaxed structure; this gives us confidence that the relaxation is reliable also for the doping series for which no experimental Sb position is available, in contrast to the well known difficulties of DFT structure prediction for iron based superconductors [42]. We model the alkali doping x by using the virtual crystal approximation for Ba, using a nuclear charge between $Z = 55$ and 56.

Appendix B: Tight binding model

We use projective Wannier functions within FPLO [32] to construct faithful tight binding models t_{ij}^{sp} of $\text{BaTi}_2\text{Sb}_2\text{O}$ and the alkali doping series:

$$H_0 = - \sum_{i,j} t_{ij}^{sp} c_{i\sigma}^\dagger c_{j\sigma} \quad (\text{B1})$$

where the t_{ij} are transfer integrals between sites i and j , s and p are orbital indices, and σ is the spin. Fig. 8 shows the quality of fit for band structure, density of states and Fermi surface of $\text{BaTi}_2\text{Sb}_2\text{O}$; the agreement

is nearly perfect. To achieve this, we need to include 26 orbitals: Ten Ti 3d orbitals, two Ti 4s orbitals, six Sb 5p orbitals, five Ba 5d orbitals and three O 2p orbitals.

Appendix C: Electronic structure

Figure 9 shows the weight of all 3d orbitals of Ti1 for $\text{BaTi}_2\text{Sb}_2\text{O}$. The Ti2 3d orbitals have weights which are 90 degree rotated with respect to Ti1 (not shown). The dominating orbital is Ti 3d_{xy}, and 3d_{xz}, 3d_{yz} orbitals have some weight at the Fermi level as well. 3d_{z²} and 3d_{x²-y²} orbitals contributions are negligibly small.

Figure 10 shows the Fermi surface of $\text{Ba}_{1-x}\text{Na}_x\text{Ti}_2\text{Sb}_2\text{O}$ at $x = 0.05$ and compares favorably with the angle resolved photoemission (ARPES) experiment of Ref. [40].

Appendix D: Spin fluctuation formalism

We consider the multiorbital Hubbard Hamiltonian [43]

$$H = H_0 + U \sum_{i,l} n_{i\uparrow} n_{i\downarrow} + \frac{U'}{2} \sum_{i,s,p \neq s} n_{is} n_{ip} - \frac{J}{2} \sum_{i,s,p \neq s} \mathbf{S}_{is} \cdot \mathbf{S}_{ip} + \frac{J'}{2} \sum_{i,s,p \neq s,\sigma} c_{i\sigma}^\dagger c_{i\bar{\sigma}}^\dagger c_{ip\bar{\sigma}} c_{ip\sigma} \quad (\text{D1})$$

with Fermionic creation (annihilation) operators $c_{i\sigma}^\dagger$ ($c_{i\sigma}$), spin operator \mathbf{S}_{is} , density operator $n_{i\sigma} = c_{i\sigma}^\dagger c_{i\sigma}$ and interaction parameters U , U' , J , J' (intraorbital Coulomb repulsion, interorbital Coulomb repulsion, Hund's rule coupling, pair-hopping term). The tight binding part H_0 is given by Eq. (B1). Diagonalization of H_0 provides band energies $E_l(\mathbf{k})$ and matrix elements a_m^s and allows calculation of the static noninteracting susceptibility

$$\chi_{st}^{pq}(\mathbf{q}) = - \sum_{\mathbf{k},l,m} a_l^{p*}(\mathbf{k}) a_l^t(\mathbf{k}) a_m^{s*}(\mathbf{k} + \mathbf{q}) a_m^q(\mathbf{k} + \mathbf{q}) \times \frac{n_F(E_l(\mathbf{k})) - n_F(E_m(\mathbf{k} + \mathbf{q}))}{E_l(\mathbf{k}) - E_m(\mathbf{k} + \mathbf{q})} \quad (\text{D2})$$

$n_F(E)$ is the Fermi distribution function. The observable static susceptibility can be calculated as

$$\chi_0(\mathbf{q}) = \frac{1}{2} \sum_{ab} \chi_{aa}^{bb}(\mathbf{q}) \quad (\text{D3})$$

Applying the random phase approximation (RPA), charge and spin susceptibilities are calculated from the noninteracting susceptibility as

$$[(\chi_c^{RPA})_{st}^{pq}]^{-1} = [\chi_{st}^{pq}]^{-1} + (U_c)_{st}^{pq} \quad (\text{D4})$$

$$[(\chi_s^{RPA})_{st}^{pq}]^{-1} = [\chi_{st}^{pq}]^{-1} - (U_s)_{st}^{pq}$$

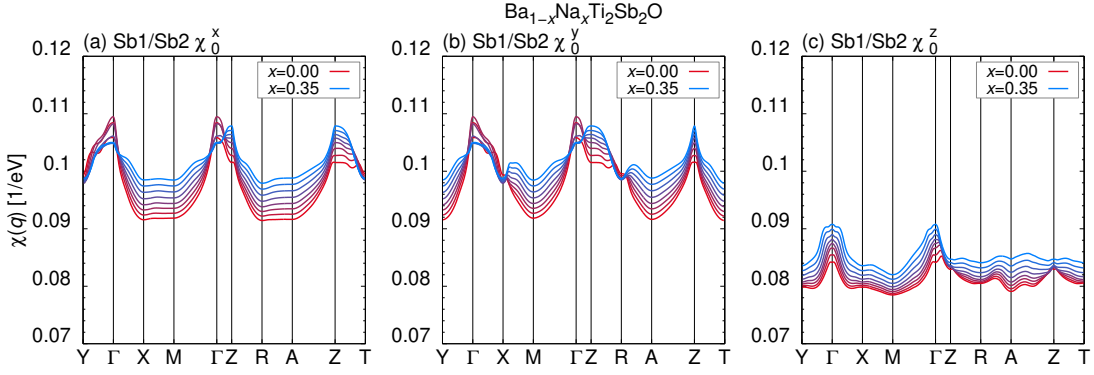


FIG. 11. Sb contribution to the non-interacting susceptibility χ_0 for $\text{Ba}_{1-x}\text{Na}_x\text{Ti}_2\text{Sb}_2\text{O}$ along a \mathbf{q} path. See Fig. 4 for the meaning of the path labels.

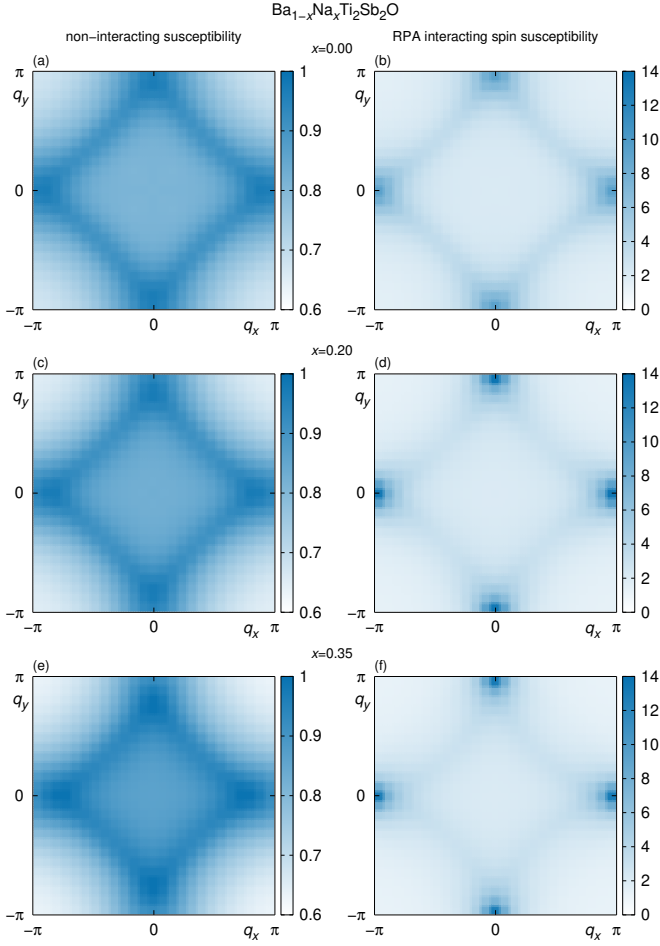


FIG. 12. Non-interacting susceptibility χ_0 and RPA interacting spin susceptibility χ_s for $\text{Ba}_{1-x}\text{Na}_x\text{Ti}_2\text{Sb}_2\text{O}$.

where nonzero components of the multi-orbital Hubbard model interaction tensors are [43]

$$\begin{aligned}
 (U_c)_{aa}^{aa} &= U & (U_c)_{bb}^{aa} &= 2U', \\
 (U_c)_{ab}^{ab} &= \frac{3}{4}J - U' & (U_c)_{ab}^{ba} &= J' \\
 (U_s)_{aa}^{aa} &= U & (U_s)_{bb}^{aa} &= \frac{1}{2}J \\
 (U_s)_{ab}^{ab} &= \frac{1}{4}J + U' & (U_s)_{ab}^{ba} &= J', \quad (\text{D5})
 \end{aligned}$$

Then, the superconducting pairing vertex in the singlet channel is

$$\begin{aligned}
 \Gamma_{st}^{pq}(\mathbf{k}, \mathbf{k}') &= \left[\frac{3}{2}U_s \chi_s^{RPA}(\mathbf{k} - \mathbf{k}') U_s + \frac{1}{2}U_s \right. \\
 &\quad \left. - \frac{1}{2}U_c \chi_c^{RPA}(\mathbf{k} - \mathbf{k}') U_c + \frac{1}{2}U_c \right]_{ps}^{tq}. \quad (\text{D6})
 \end{aligned}$$

This vertex in orbital space is projected onto band space using the eigenvectors of H_0 ,

$$\begin{aligned}
 \Gamma_{ij}(\mathbf{k}, \mathbf{k}') &= \sum_{s,t,p,q} a_i^{t*}(-\mathbf{k}) a_i^{s*}(\mathbf{k}) \text{Re} [\Gamma_{st}^{pq}(\mathbf{k}, \mathbf{k}')] a_j^p(\mathbf{k}') a_j^q(-\mathbf{k}'). \quad (\text{D7})
 \end{aligned}$$

and the gap equation

$$\begin{aligned}
 - \sum_j \oint_{C_j} \frac{dk'_{\parallel}}{2\pi} \frac{1}{4\pi v_F(\mathbf{k}')} [\Gamma_{ij}(\mathbf{k}, \mathbf{k}') + \Gamma_{ij}(\mathbf{k}, -\mathbf{k}')] g_j(\mathbf{k}') \\
 = \lambda_i g_i(\mathbf{k}) \quad (\text{D8})
 \end{aligned}$$

is solved for the pairing eigenvalue λ_i and the gap function $g_i(\mathbf{k})$.

Appendix E: Susceptibility

The evolution of the Sb $5p_x$, $5p_y$ and $5p_z$ contributions to the non-interacting susceptibility of

$\text{Ba}_{1-x}\text{Na}_x\text{Ti}_2\text{Sb}_2\text{O}$ with doping level x is shown in Fig. 11. The values of the susceptibilities compared to Ti $3d$ orbitals are small (see scale of Fig. 4), and their variation with \mathbf{q} value is tiny. With doping, the three susceptibilities grow even more featureless.

The non-interacting susceptibility χ_0 and RPA interacting spin susceptibility χ_s is shown in Fig. 12. This is based on a 3D calculation of χ_0 on a $25 \times 25 \times 9$ grid using a $25 \times 25 \times 9$ integration grid. The $q_z = 0$ cut shown in Fig. 12 is extracted using a 100×100 interpolation grid. The same interpolation grid was used for the interacting susceptibility χ_s shown in the main text, Fig.

5 (a).

ACKNOWLEDGMENTS

We acknowledge fruitful discussions with Yoshihiro Kubozono. Part of the computations were carried out at the Supercomputer Center at the Institute for Solid State Physics, the University of Tokyo. This work was supported by MEXT Leading Initiative for Excellent Young Researchers.

-
- [1] A. Adam and H.-U. Schuster, Darstellung und kristallstruktur der pnictidoxide $\text{Na}_2\text{Ti}_2\text{As}_2\text{O}$ und $\text{Na}_2\text{Ti}_2\text{Sb}_2\text{O}$, *Z. Anorg. Allg. Chem.* **584**, 150 (1990).
- [2] E. Axtell, T. Ozawa, S. M. Kauzlarich, and R. R. Singh, Phase transition and spin-gap behavior in a layered tetragonal pnictide oxide, *J. Solid State Chem.* **134**, 423 (1997).
- [3] W. E. Pickett, Electronic instability in inverse- K_2NiF_4 -structure $\text{Na}_2\text{Sb}_2\text{Ti}_2\text{O}$, *Phys. Rev. B* **58**, 4335 (1998).
- [4] T. Yajima, K. Nakano, F. Takeiri, T. Ono, Y. Hosokoshi, Y. Matsushita, J. Hester, Y. Kobayashi, and H. Kageyama, Superconductivity in $\text{BaTi}_2\text{Sb}_2\text{O}$ with a d^1 square lattice, *J. Phys. Soc. Jpn.* **81**, 103706 (2012).
- [5] T. Yajima, K. Nakano, F. Takeiri, J. Hester, T. Yamamoto, Y. Kobayashi, N. Tsuji, J. Kim, A. Fujiwara, and H. Kageyama, Synthesis and physical properties of the new oxybismuthides $\text{BaTi}_2\text{Bi}_2\text{O}$ and $(\text{SrF})_2\text{Ti}_2\text{Bi}_2\text{O}$ with a d^1 square net, *J. Phys. Soc. Jpn.* **82**, 013703 (2013).
- [6] T. Yajima, K. Nakano, F. Takeiri, Y. Nozaki, Y. Kobayashi, and H. Kageyama, Two superconducting phases in the isovalent solid solutions $\text{BaTi}_2Pn_2\text{O}$ ($Pn = \text{As, Sb, and Bi}$), *J. Phys. Soc. Jpn.* **82**, 033705 (2013).
- [7] H.-F. Zhai, W.-H. Jiao, Y.-L. Sun, J.-K. Bao, H. Jiang, X.-J. Yang, Z.-T. Tang, Q. Tao, X.-F. Xu, Y.-K. Li, C. Cao, J.-H. Dai, Z.-A. Xu, and G.-H. Cao, Superconductivity, charge- or spin-density wave, and metal-nonmetal transition in $\text{BaTi}_2(\text{Sb}_{1-x}\text{Bi}_x)_2\text{O}$, *Phys. Rev. B* **87**, 100502(R) (2013).
- [8] X. F. Wang, Y. J. Yan, J. J. Ying, Q. J. Li, M. Zhang, N. Xu, and X. H. Chen, Structure and physical properties for a new layered pnictide-oxide: $\text{BaTi}_2\text{As}_2\text{O}$, *J. Phys.: Condens. Matter* **22**, 075702 (2010).
- [9] P. Doan, M. Gooch, Z. Tang, B. Lorenz, A. Möller, J. Tapp, P. C. W. Chu, and A. M. Guloy, $\text{Ba}_{1-x}\text{Na}_x\text{Ti}_2\text{Sb}_2\text{O}$ ($0.0 \leq x \leq 0.33$): A layered titanium-based pnictide oxide superconductor, *J. Am. Chem. Soc.* **134**, 16520 (2012).
- [10] R. H. Liu, D. Tan, Y. A. Song, Q. J. Li, Y. J. Yan, J. J. Ying, Y. L. Xie, X. F. Wang, and X. H. Chen, Physical properties of the layered pnictide oxides $\text{Na}_2\text{Ti}_2P_2\text{O}$ ($P=\text{As, Sb}$), *Phys. Rev. B* **80**, 144516 (2009).
- [11] S. Kitagawa, K. Ishida, K. Nakano, T. Yajima, and H. Kageyama, s -wave superconductivity in superconducting $\text{BaTi}_2\text{Sb}_2\text{O}$ revealed by $^{121/123}\text{Sb}$ -NMR/nuclear quadrupole resonance measurements, *Phys. Rev. B* **87**, 060510(R) (2013).
- [12] F. von Rohr, A. Schilling, R. Nesper, C. Baines, and M. Bendele, Conventional superconductivity and charge-density-wave ordering in $\text{Ba}_{1-x}\text{Na}_x\text{Ti}_2\text{Sb}_2\text{O}$, *Phys. Rev. B* **88**, 140501(R) (2013).
- [13] Y. Nozaki, K. Nakano, T. Yajima, H. Kageyama, B. Frandsen, L. Liu, S. Cheung, T. Goko, Y. J. Uemura, T. S. J. Munsie, T. Medina, G. M. Luke, J. Munevar, D. Nishio-Hamane, and C. M. Brown, Muon spin relaxation and electron/neutron diffraction studies of $\text{BaTi}_2(\text{As}_{1-x}\text{Sb}_x)_2\text{O}$: Absence of static magnetism and superlattice reflections, *Phys. Rev. B* **88**, 214506 (2013).
- [14] U. Pachmayr and D. Johrendt, Superconductivity in $\text{Ba}_{1-x}\text{K}_x\text{Ti}_2\text{Sb}_2\text{O}$ ($0 \leq x \leq 1$) controlled by the layer charge, *Solid State Sci.* **28**, 31 (2014).
- [15] F. von Rohr, R. Nesper, and A. Schilling, Superconductivity in rubidium-substituted $\text{Ba}_{1-x}\text{Rb}_x\text{Ti}_2\text{Sb}_2\text{O}$, *Phys. Rev. B* **89**, 094505 (2014).
- [16] Y. Wang, X. Yang, T. Taguchi, H. Li, T. He, H. Goto, R. Eguchi, T. Miyazaki, Y.-F. Liao, H. Ishii, and Y. Kubozono, Preparation and characterization of superconducting $\text{Ba}_{1-x}\text{Cs}_x\text{Ti}_2\text{Sb}_2\text{O}$, and its pressure dependence of superconductivity, *Jpn. J. Appl. Phys.* **58**, 110603 (2019).
- [17] W. Ishii, T. Yajima, and Z. Hiroi, Electronic phase diagram of the titanium oxypnictide superconductor $\text{BaTi}_2(\text{Sb}_{1-x}\text{Bi}_x)_2\text{O}$, *J. Phys.: Conf. Ser.* **969**, 012052 (2018).
- [18] Y. Wang, H. Li, T. Taguchi, A. Suzuki, A. Miura, H. Goto, R. Eguchi, T. Miyazaki, Y.-F. Liao, H. Ishii, and Y. Kubozono, Superconducting behavior of $\text{BaTi}_2\text{Bi}_2\text{O}$ and its pressure dependence, *Phys. Chem. Chem. Phys.* **22**, 23315 (2020).
- [19] B. Lorenz, A. M. Guloy, and P. C. W. Chu, Superconductivity in titanium-based pnictide oxide compounds, *Int. J. Mod. Phys. B* **28**, 1430011 (2014).
- [20] M. Gooch, P. Doan, Z. Tang, B. Lorenz, A. M. Guloy, and P. C. W. Chu, Weak coupling BCS-like superconductivity in the pnictide oxide $\text{Ba}_{1-x}\text{Na}_x\text{Ti}_2\text{Sb}_2\text{O}$ ($x = 0$ and 0.15), *Phys. Rev. B* **88**, 064510 (2013).
- [21] S. Kamusella, P. Doan, T. Goltz, H. Luetkens, R. Sarkar, A. Guloy, and H.-H. Klauss, CDW order and unconventional s -wave superconductivity in $\text{Ba}_{1-x}\text{Na}_x\text{Ti}_2\text{Sb}_2\text{O}$, *J. Phys.: Conf. Ser.* **551**, 012026 (2014).

- [22] S. Kitagawa, K. Ishida, W. Ishii, T. Yajima, and Z. Hiroi, Nematic transition and highly two-dimensional superconductivity in $\text{BaTi}_2\text{Bi}_2\text{O}$ revealed by ^{209}Bi -nuclear magnetic resonance/nuclear quadrupole resonance measurements, *Phys. Rev. B* **98**, 220507(R) (2018).
- [23] A. Subedi, Electron-phonon superconductivity and charge density wave instability in the layered titanium-based pnictide $\text{BaTi}_2\text{Sb}_2\text{O}$, *Phys. Rev. B* **87**, 054506 (2013).
- [24] D. J. Singh, Electronic structure, disconnected Fermi surfaces and antiferromagnetism in the layered pnictide superconductor $\text{Na}_x\text{Ba}_{1-x}\text{Ti}_2\text{Sb}_2\text{O}$, *New J. Phys.* **14**, 123003 (2012).
- [25] G. Zhang, J. K. Glasbrenner, R. Flint, I. I. Mazin, and R. M. Fernandes, Double-stage nematic bond ordering above double stripe magnetism: Application to $\text{BaTi}_2\text{Sb}_2\text{O}$, *Phys. Rev. B* **95**, 174402 (2017).
- [26] X.-L. Yu, D.-Y. Liu, Y.-M. Quan, T. Jia, H.-Q. Lin, and L.-J. Zou, A site-selective antiferromagnetic ground state in layered pnictide-oxide $\text{BaTi}_2\text{As}_2\text{O}$, *J. Appl. Phys.* **115**, 17A924 (2014).
- [27] H. Kim, J. H. Shim, K. Kim, and B. I. Min, Charge density waves and the Coulomb correlation effects in $\text{Na}_2\text{Ti}_2\text{P}_2\text{O}$ ($P=\text{Sb}, \text{As}$), *Phys. Rev. B* **96**, 155142 (2017).
- [28] G. Wang, H. Zhang, L. Zhang, and C. Liu, The electronic structure and magnetism of $\text{BaTi}_2\text{Sb}_2\text{O}$, *J. Appl. Phys.* **113**, 243904 (2013).
- [29] X.-W. Yan and Z.-Y. Lu, Layered pnictide-oxide $\text{Na}_2\text{Ti}_2\text{Pn}_2\text{O}$ ($\text{Pn}=\text{As}, \text{Sb}$): a candidate for spin density waves, *J. Phys.: Condens. Matter* **25**, 365501 (2013).
- [30] K. Koepnik and H. Eschrig, Full-potential nonorthogonal local-orbital minimum-basis band-structure scheme, *Phys. Rev. B* **59**, 1743 (1999).
- [31] J. P. Perdew, K. Burke, and M. Ernzerhof, Generalized gradient approximation made simple, *Phys. Rev. Lett.* **77**, 3865 (1996).
- [32] H. Eschrig and K. Koepnik, Tight-binding models for the iron-based superconductors, *Phys. Rev. B* **80**, 104503 (2009).
- [33] D. Guterding, H. O. Jeschke, P. J. Hirschfeld, and R. Valentí, Unified picture of the doping dependence of superconducting transition temperatures in alkali metal/ammonia intercalated FeSe, *Phys. Rev. B* **91**, 041112(R) (2015).
- [34] D. Guterding, *Microscopic modelling of organic and iron-based superconductors*, Ph.D. thesis, Goethe-Universität Frankfurt, Germany (2017).
- [35] M. Shimizu, N. Takemori, D. Guterding, and H. O. Jeschke, Two-dome superconductivity in FeS induced by a Lifshitz transition, *Phys. Rev. Lett.* **121**, 137001 (2018).
- [36] M. Shimizu, N. Takemori, D. Guterding, and H. O. Jeschke, Importance of the Fermi surface and magnetic interactions for the superconducting dome in electron-doped FeSe intercalates, *Phys. Rev. B* **101**, 180511(R) (2020).
- [37] H. Hosono, K. Tanabe, E. Takayama-Muromachi, H. Kageyama, S. Yamanaka, H. Kumakura, M. Nohara, H. Hiramatsu, and S. Fujitsu, Exploration of new superconductors and functional materials, and fabrication of superconducting tapes and wires of iron pnictides, *Sci. Technol. Adv. Mater.* **16**, 033503 (2015).
- [38] H. Nakaoka, Y. Yamakawa, and H. Kontani, Theoretical prediction of nematic orbital-ordered state in the Ti oxypnictide superconductor $\text{BaTi}_2(\text{As}, \text{Sb})_2\text{O}$, *Phys. Rev. B* **93**, 245122 (2016).
- [39] D. W. Song, J. Li, D. Zhao, L. K. Ma, L. X. Zheng, S. J. Li, L. P. Nie, X. G. Luo, Z. P. Yin, T. Wu, and X. H. Chen, Revealing the hidden order in $\text{BaTi}_2\text{As}_2\text{O}$ via nuclear magnetic resonance, *Phys. Rev. B* **98**, 235142 (2018).
- [40] N. R. Davies, R. D. Johnson, A. J. Princep, L. A. Gannon, J.-Z. Ma, T. Qian, P. Richard, H. Li, M. Shi, H. Nowell, P. J. Baker, Y. G. Shi, H. Ding, J. Luo, Y. F. Guo, and A. T. Boothroyd, Coupled commensurate charge density wave and lattice distortion in $\text{Na}_2\text{Ti}_2\text{Pn}_2\text{O}$ ($\text{Pn}=\text{As}, \text{Sb}$) determined by x-ray diffraction and angle-resolved photoemission spectroscopy, *Phys. Rev. B* **94**, 104515 (2016).
- [41] Z. Huang, W. L. Liu, H. Y. Wang, Y. L. Su, Z. T. Liu, X. B. Shi, S. Y. Gao, Z. C. Jiang, Z. H. Liu, J. S. Liu, X. L. Lu, Y. C. Yang, J. X. Zhang, S. C. Huan, W. Xia, J. H. Wang, Y. S. Wu, X. Wang, N. Yu, Y. B. Huang, S. Qiao, J. Li, W. W. Zhao, Y. F. Guo, G. Li, and D. W. Shen, Dual topological superconducting states in the layered titanium-based oxypnictide superconductor $\text{BaTi}_2\text{Sb}_2\text{O}$ (2020), arXiv:2009.06805.
- [42] I. I. Mazin, M. D. Johannes, L. Boeri, K. Koepnik, and D. J. Singh, Problems with reconciling density functional theory calculations with experiment in ferropnictides, *Phys. Rev. B* **78**, 085104 (2008).
- [43] S. Graser, T. A. Maier, P. J. Hirschfeld, and D. J. Scalapino, Near-degeneracy of several pairing channels in multiorbital models for the Fe pnictides, *New J. Phys.* **11**, 025016 (2009).